Available online at www.sciencedirect.com
ScienceDirect
Journal of Catalysis 247 (2007) 256–268
JOURNAL OF CATALYSIS
www.elsevier.com/locate/jcat

Silica- and titania-supported Ni–Au: Application in catalytic hydrodechlorination

Guang Yuan [a], Catherine Louis [b], Laurent Delannoy [b], Mark A. Keane [c,*]

[a] *Department of Chemical and Materials Engineering, University of Kentucky, Lexington, KY, USA*
[b] *Laboratoire de Réactivité de Surface, UMR 7609 CNRS, Université Pierre et Marie Curie, 4 place Jussieu, 75252 Paris Cedex 05, France*
[c] *Chemical Engineering, School of Engineering and Physical Sciences, Heriot–Watt University, Edinburgh EH14 4AS, Scotland, UK*

Received 16 November 2006; revised 19 January 2007; accepted 8 February 2007

Abstract

The catalytic gas-phase (473 K) hydrodechlorination (HDC) of 2,4-dichlorophenol has been investigated over Ni/SiO_2, Ni/TiO_2, $Ni–Au/SiO_2$, and $Ni/Au–TiO_2$ (Ni loading ca. 5 wt%; bulk Ni/Au atomic ratio = 10). The samples were prepared by either (co-)impregnation or (co-)deposition–precipitation. The catalyst samples were characterized in terms of BET surface area, TPR, H_2 chemisorption, and TEM-EDX measurements. The impregnated Ni/SiO_2 and Ni/TiO_2 samples had a similar narrow Ni particle size distribution (1–6 nm). The addition of Au to both Ni/support samples lowered the temperature requirements for Ni^{II} reduction and suppressed H_2 chemisorption. The impregnated $Ni–Au/SiO_2$ (10–150 nm) and $Ni–Au/TiO_2$ (2–95 nm) were characterized by a wider range of particle sizes than the monometallic nickel catalysts and a variable surface Ni/Au atomic ratio (<1–40). In comparison, $Ni–Au/TiO_2$ prepared by deposition–precipitation exhibited a narrower particle size range (2–60 nm) and a more uniform Ni and Au surface distribution (Ni/Au atomic ratio of <1–15). The titania-supported catalysts delivered significantly higher specific HDC rates and distinct HDC selectivities than the silica systems, with catalytic responses discussed in terms of metal–support and reactant–surface interactions. The incorporation of Au, regardless of the support or method of preparation, resulted in higher HDC activity, an effect attributed to a surface Ni–Au synergism. Hydrogen thermal treatment of the bimetallic catalysts after reaction resulted in appreciable surface reconstruction, notably a more homogeneous combination of Ni and Au in smaller particles, which enhanced HDC performance.

Keywords: Hydrodechlorination; 2,4-Dichlorophenol; $Ni–Au/TiO_2$; $Ni–Au/SiO_2$

1. Introduction

In response to experimental evidence of high activity in the low-temperature oxidation of CO over oxide-supported Au [1], the use of Au in heterogeneous catalysis has attracted appreciable research interest [2–4]. The potential application of Au-based catalysts in various environmental remediation systems has been considered [5,6]. In earlier work [7], we demonstrated the efficacy of silica-supported Ni–Au in promoting the hydrogen-mediated dechlorination of chloro-organic pollutants. Although Au delivers lower hydrogenation rates compared with conventional Pd, Ni, and Pt catalysts [8], the application of Au catalysts when hydrogenation selectivity is critical shows much promise. Well-dispersed Au on Al_2O_3 (Au particle size, ca. 3 nm) has been used to promote the partial hydrogenation of acetylene to ethylene with 100% selectivity over the temperature range of 313–523 K [9]. In addition, Au/Al_2O_3, Au/SiO_2, and Au/TiO_2 have exhibited 100% selectivity to butenes with 50–70% selectivity to 1-butene for the hydrogenation (at 415–458 K) of 1,3-butadiene [10]. In the hydrogenation of crotonaldehyde over Au/TiO_2, smaller supported Au particles (ca. 2 nm diameter) delivered turnover frequencies up to seven times greater than that associated with larger Au particles (4–9 nm) [11]. Whereas the activity of Au/TiO_2 was two orders of magnitude lower than that of Pt/TiO_2, the Au catalyst generated a significantly higher selectivity with respect to crotyl alcohol as the target product.

An alternative approach to enhancing activity while retaining selectivity lies in the design of Au-based bimetallic cata-

* Corresponding author.
E-mail address: m.a.keane@hw.ac.uk (M.A. Keane).

0021-9517/$ – see front matter
doi:10.1016/j.jcat.2007.02.008

lysts, in which a synergetic effect between gold and the second metal can occur [12]. Taking acetylene hydrogenation as an example of this effect, a Pd-promoted Au/TiO_2 catalyst exhibited significantly higher ethylene selectivity and stability compared with Pd/TiO_2 [13]. In the hydrodechlorination (HDC) of dichlorodifluoromethane (CFC-12), Pd–Au/C showed enhanced selectivity to CH_2F_2 (87%) relative to Pd/C (72%) at 453 K, where the formation of a Pd–Au alloy was linked to this superior selectivity [14–16]; this effect was shown to extend to silica-supported Pd–Au [16]. Enhanced HDC of trichloroethene also has been reported for Pd supported on Au nanoparticles and Pd-impregnated Au/Al_2O_3 [17], and Au promotion of hydrodesulfurization has been demonstrated for silica-supported Au–Pd [18].

There is a dearth of literature dealing with the catalytic implications of Ni–Au combinations, which is the focus of this study. However, Molenbroek et al. [19,20] have reported improved time-on-stream (TOS) performance for $Ni–Au/SiO_2$ relative to Ni/SiO_2 in butane steam reforming, where the formation of a Ni–Au surface alloy was proposed to limit coke deposition and thus prolong catalytic activity. Triantafyllopoulos and Neophytides [21] have also noted that the addition of Au to Ni/YSZ served to suppress carbon deposition during methane steam reforming. In an earlier study [7], we demonstrated that $Ni–Au/SiO_2$ delivered higher activity than Ni/SiO_2 in the gas-phase hydrodechlorination (HDC) of 2,4-dichlorophenol (2,4-DCP), a response that we linked to the creation of surface Ni–Au interactions. Catalytic HDC represents an innovative methodology for transforming toxic hazardous chloro-aromatic waste into recyclable products [22]. Chlorophenols, the focus of this study, are commercially important chemicals used as end products and intermediates in the manufacture of herbicides, dyes, and plant growth regulators [23], but are also persistent toxic compounds for which the environment has little assimilative capacity [24]. Catalytic HDC offers a controlled H_2 cleavage of one or more C–Cl bonds, lowering toxicity and generating reusable raw material from chlorophenolic waste. Moreover, in earlier studies catalytic HDC has served as an effective test reaction to probe hydrogenolytic activity and selectivity for supported Ni catalysts [25–29].

In this report, we have extended the earlier study of $Ni–Au/SiO_2$ to consider the action of Ni/TiO_2, Au/TiO_2, and $Ni–Au/TiO_2$ (5 wt% Ni and Ni/Au [at:at] = 10), comparing the impact of the support (TiO_2 vs SiO_2) in determining Au–Ni surface synergism. We link critical catalyst characteristics (from BET, TPR, H_2 chemisorption, and TEM-EDX analyses) to catalytic HDC data. We also address the role of catalyst preparation by examining impregnation and deposition–precipitation as two distinct synthetic routes to titania-supported Ni–Au.

2. Experimental

2.1. Catalyst preparation

Two supports were used: silica XOA400, from Rhodia (356 $m^2\,g^{-1}$; pore volume, 1.25 $cm^3\,g^{-1}$; average pore diameter, 8 nm), and TiO_2 P25, from Degussa (45 $m^2\,g^{-1}$; nonporous; primary particle size, ca. 21 nm). Ni-loaded SiO_2 and TiO_2 (5 wt%) were prepared using the same method used in our earlier study [7], that is, impregnation with a solution of $[Ni(en)_3](NO_3)_2$ (0.43 M, 2 $cm^3\,g^{-1}_{support}$); the impregnated samples are denoted by the suffix "-IMP." The Ni precursor was prepared by mixing 20 cm^3 of 1 M aqueous $Ni(NO_3)_2$ with 5 cm^3 of ethanediamine (99%), en/Ni $\geqslant$ 3. This route to supported Ni is known to lead to small supported Ni particles (after reduction) for Ni loadings up to 20 wt% [29]. Au/SiO_2 and Au/TiO_2 (1.7 ± 0.1 wt%) were prepared by impregnation with a 0.04 M aqueous solution of $[Au(en)_2]Cl_3$ (2 cm^3/g), which was synthesized according to the method of Block and Bailar [30]. Au–Ni-loaded TiO_2 (5 wt% Ni and Ni/Au [at:at] = 10) was prepared using two different methods, co-impregnation and co-deposition–precipitation. The latter approach is used here for the first time for the preparation of supported Au–Ni but is known to facilitate a high dispersion of Ni on silica [31] and Au on titania [32]. Au–Ni-loaded SiO_2 was prepared only by co-impregnation, because deposition–precipitation of gold on silica is not possible due to the low point of zero charge (ca. 2) of the silica support [33,34]. For the co-impregnated Au–Ni on TiO_2 and SiO_2, an appropriate amount of $[Au(en)_2]Cl_3$ (0.04 M) was dissolved in the $[Ni(en)_3](NO_3)_2$ solution (0.43 M) and used to impregnate the silica and titania supports (2 $cm^3\,g^{-1}$ SiO_2 or TiO_2), to achieve a Ni/Au atomic ratio of 10. The titania-supported bimetallic prepared by co-deposition–precipitation is denoted by the suffix "-DP." This synthesis route involves the precipitation of both metals onto the support (1 g) from an aqueous solution (100 cm^3) of $HAuCl_4$ (8.5×10^{-4} M) and $Ni(NO_3)_2$ (8.5×10^{-3} M) by a basification of the support/salt solution suspension through the decomposition of urea (0.42 M) at 353 K for 20 h. In addition, a Au/TiO_2–DP sample was prepared by deposition/precipitation of $HAuCl_4$ with urea using the same procedure, as described in detail elsewhere [32,38]. The impregnated samples were aged at room temperature for 1 h and dried under vacuum at 373 K for 2 h; then each sample was sieved into a batch of 75 μm average particle diameter.

2.2. Techniques

The metal loadings were determined (to within ±2%) by inductively coupled plasma-optical emission spectrometry (ICP-OES; Vista-PRO, Varian) from the diluted extract of aqua regia. Temperature-programmed reduction (TPR), H_2 chemisorption, and BET surface area were determined using the commercial CHEM-BET 3000 (Quantachrome) unit; BJH pore volume analyses were performed using the commercial Micromeritics TriStar 3000 unit. The as-prepared catalysts (ca. 0.1 g) were loaded into a U-shaped Pyrex glass cell (10 cm × 3.76 mm i.d.) and contacted at room temperature with a 20 $cm^3\,min^{-1}$ (mass flow controlled) 5% v/v H_2/N_2 flow for 0.5 h before heating at 2 $K\,min^{-1}$ to the final reduction temperature with the effluent gas directed through a liquid N_2 trap. H_2 consumption was monitored by a thermal conductivity detector with data acquisition/manipulation using the TPR Win software. The reduced samples were swept with a 20 $cm^3\,min^{-1}$ flow of N_2 for 1 h,

cooled to room temperature, and subjected to H_2 chemisorption using a pulse (50 μl) titration procedure. Total surface area was recorded in a 30% v/v N_2/He flow, with pure N_2 (99.9%) as the internal standard.

After outgassing for 30 min, at least two cycles of N_2 adsorption–desorption in the flow mode were performed, using the standard single-point BET method. The BET surface areas and H_2 uptake values were reproducible to within ±5%; the values quoted in this paper are the mean. Metal particle size and surface composition were determined by transmission electron microscopy (TEM) using a JEOL 2000 TEM microscope equipped with a UTW energy-dispersive X-ray (EDX) detector (Oxford Instruments) and operating at an accelerating voltage of 200 kV. The catalyst sample was dispersed in 1-butanol by ultrasonic vibration and deposited on a lacey-carbon/Cu grid (200 Mesh), then dried at 383 K for 1 h. Surface analyses were also conducted by high-resolution transmission electron microscopy (HRTEM) using a JEOL-2010 TEM/STEM, with transient EDX mapping (1 nm s^{-1}) conducted over selected sample lengths.

Before reaction, the as-prepared IMP and DP catalysts were activated by heating in 60 cm^3 min^{-1} dry H_2 (99.999%) at a rate of 2 K min^{-1} to 603 and 773 K, respectively, and maintaining these temperatures for 4 h. These activation conditions match those used before sample characterization. The reactions were conducted under atmospheric pressure in a fixed-bed glass reactor (15 mm i.d.) with a co-current flow of the aromatic feed in ultrapure H_2 (GHSV $= 2.1 \times 10^4$; $T = 473$ K). A layer of glass beads above the catalyst bed ensured that the reactants were vaporized and reached the reaction temperature before contacting the catalyst. A kd Scientific model 100 microprocessor-controlled infusion pump was used to deliver the feed through a glass/Teflon airtight syringe and Teflon line at a fixed calibrated flow rate. The reactor and operating conditions to ensure negligible heat/mass transport limitations have been described in detail elsewhere [25,26]. HDC performance was assessed over two reaction cycles at $W_{Ni}/F_{Cl} = 500$–3000 g_{Ni} mol_{Cl}^{-1} min and $W_{Au}/F_{Cl} = 160$–1000 g_{Au} mol_{Cl}^{-1} min, where W_{Ni} (W_{Au}) is the mass of Ni (Au) in the catalyst bed and F_{Cl} is the inlet Cl molar flow rate. In the first cycle, after catalyst activation, the HDC reaction was conducted for 8 h at 473 K, followed by regeneration in H_2 at 603 K for 12 h and then a second HDC cycle conducted for 8 h at 473 K. A halogen (in the form of HCl product) mass balance was performed by passing the effluent gas through an aqueous NaOH (3.5–8.0×10^{-3} mol dm^{-3}, kept under constant agitation at ⩾300 rpm) trap while continuously monitoring the pH by means of a Hanna HI programmable printing pH benchmeter. The concentration of HCl generated was also measured by titrimetric analysis of the NaOH trap solution using a Metrohm model 728 autotitrator ($AgNO_3$, combined Ag electrode); Cl mass balance was complete to better than ±8%. The reaction products were analyzed by capillary gas chromatography as described elsewhere [35]; the detection limit corresponded to a feedstock conversion of <0.4 mol%, and the overall analytic reproducibility was better than ±2%. The degree of HDC (x_{Cl}) is given by $[HCl]_{out}/[Cl_{org}]_{in}$, where $[Cl_{org}]$ represents the Cl concentration (mol dm^{-3}) associated with the 2,4-DCP feed, and the selectivity with which a partially dechlorinated CP is produced from 2,4-DCP can be calculated from

$$S_{CP} = \frac{[CP]_{out}}{[2,4-DCP]_{in} - [2,4-DCP]_{out}} \times 100,$$

where in and out refer to the inlet and outlet reactor streams, respectively. In a series of blank tests, passage of each reactant in a stream of H_2 through the empty reactor (i.e., in the absence of catalyst) did not result in any detectable conversion. Repeated catalytic runs with different samples from the same batch of catalyst delivered product compositions that were reproducible to within ±6%.

3. Results and discussion

3.1. Catalyst characterization before reaction

The metal loadings, bulk Ni/Au ratios, and associated BET surface areas of the activated passivated samples are recorded in Table 1. The BET areas of the metal-loaded SiO_2 samples were somewhat lower than that of the SiO_2 support (356 m^2 g^{-1}), which can be attributed to partial pore blocking; for example, Ni/SiO_2–IMP exhibited a ca. 10% decrease in pore volume (1.13 cm^3 g^{-1}) relative to the support. The BET surface areas of the TiO_2 systems were unaffected by the incorporation of Ni and/or Au and were close to that of the starting TiO_2 (45 m^2 g^{-1}). The TPR profiles generated for the reduction of the as-prepared Ni/TiO_2–IMP (profile I) and Ni/SiO_2–IMP (profile II) are given in Fig. 1a. Both profiles are featureless up to ca. 520 K with a subsequent broad region of H_2 consumption extending into the final isothermal hold at 603 K with an ultimate return to baseline.

Previous studies have demonstrated that an [en]/[Ni^{II}] ratio >3 results in a supported $[Ni(en)_3]^{2+}$ that is fully reduced at 603 K to Ni^0 [36]. Hydrogen consumption during the reduction of ethanediamine-containing precursors has been shown to far exceed the H_2 required for Ni^{II} to Ni^0 reduction, a response that can be attributed to a Ni-catalyzed hydrogenolysis of the amine [7]. Indeed, total H_2 consumption during TPR of both monometallic catalysts represents a H_2/Ni mol ratio of 11, in good agreement with that reported previously in Ref. [36]. The TPR profiles for Au/TiO_2–IMP (profile III) and Au/SiO_2–IMP

Table 1
Ni and Au contents and BET areas of the catalysts prepared by (co-)impregnation (-IMP) and (co-)deposition–precipitation (-DP)

Catalyst	Ni content (% w/w)	Au content (% w/w)	Ni/Au (mol/mol)	BET area (m^2 g^{-1})
Ni/TiO_2–IMP	5.0	–	–	44
Au/TiO_2–IMP	–	1.6	–	42
Au/TiO_2–DP	–	1.8	–	40
Ni–Au/TiO_2–IMP	4.7	1.6	9.9	41
Ni–Au/TiO_2–DP	5.7	2.0	9.6	40
Ni/SiO_2–IMP	5.1	–	–	336
Au/SiO_2–IMP	–	1.7	–	333
Ni–Au/SiO_2–IMP	4.9	1.6	10.2	325

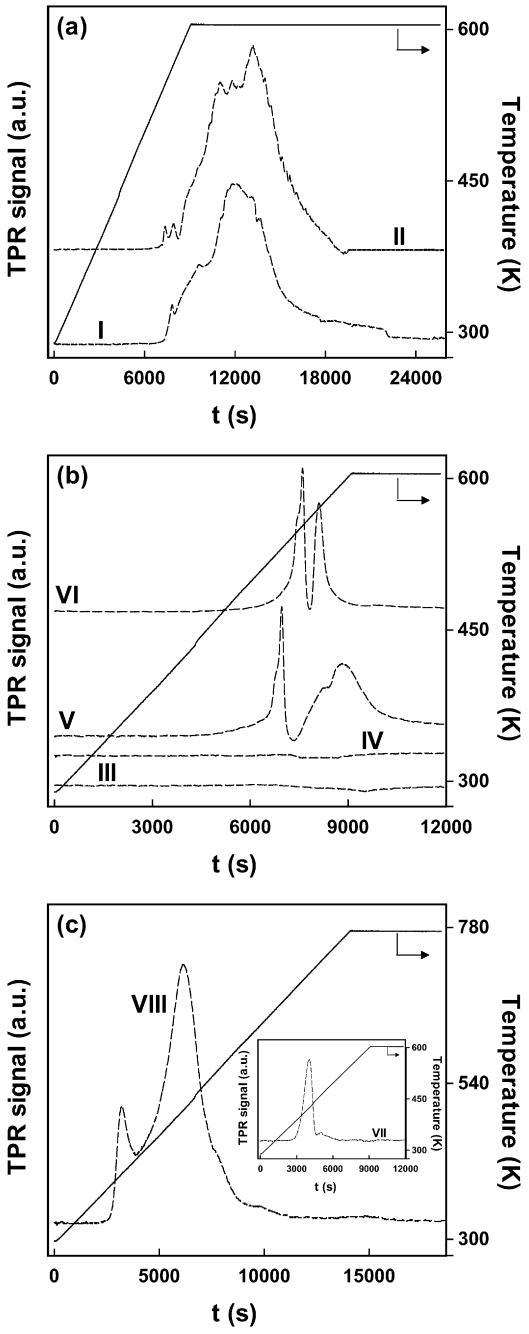

Fig. 1. Temperature-programmed reduction (TPR) profiles for (a) Ni/TiO_2–IMP (I), Ni/SiO_2–IMP (II), (b) Au/TiO_2–IMP (III), Au/SiO_2–IMP (IV), Ni–Au/TiO_2–IMP (V), Ni–Au/SiO_2–IMP (VI), (c) Au/TiO_2–DP (VII) and Ni–Au/TiO_2–DP (VIII).

(profile IV) given in Fig. 1b show no detectable H_2 consumption. It has been demonstrated [37] in the case of a zeolite-supported gold catalyst that $[Au(en)_2]^{3+}$ decomposes when heated above 313 K, and the gold is reduced by the ethanediamine ligands. After impregnation, our samples were dried at 373 K, which may have caused a temperature-induced decomposition of the gold ethanediamine precursor into metallic gold.

We have also reported that when $[Au(en)_2]^{3+}$ cation adsorption on titania was performed at 323 K, gold reduced in solution [38]. In marked contrast, the TPR profile for Au/TiO_2–DP (profile VII in Fig. 1c) exhibited a sharp H_2 consumption peak at 415 K with an associated H_2/Au mol ratio of 1.6. This result confirms that in sample preparation by deposition–precipitation with urea, gold was not reduced during the drying step, and thus we assign the observed H_2 consumption principally to the reduction of supported gold.

Two sharp peaks characterize the TPR profiles (see Fig. 1b) generated for Ni–Au/TiO_2–IMP (at 518 and 585 K, profile V) and Ni–Au/SiO_2–IMP (at 536 and 552 K, profile VI). Comparing this TPR response with the profiles shown in Fig. 1a for the monometallic catalysts apparently shows that the inclusion of Au influences TPR behavior, rendering the Ni^{II} component on both oxide supports more susceptible to reduction. Although we could not find any directly comparable TPR analysis in the literature, we can flag the work of Triantafyllopoulos and Neophytides [21], who found that Au-modified Ni/YSZ samples were reduced at temperatures 150 K lower than those required for the reduction of Ni/YSZ. Moreover, a decrease (by up to 140 K) in the temperature of reduction of Fe_2O_3 to Fe_3O_4 has been reported [39,40], due to the addition of Au, an effect that extends to the reduction of ceria in Au/CeO_2 [41] and Au-V_2O_5/CeO_2 [42]. Reduction of Ni–Au/TiO_2–DP (see profile VIII in Fig. 1c) also generated two peaks, at 410 K and 500 K. The former peak coincides with the TPR response for Au/TiO_2–DP, whereas the latter can be ascribed to the reduction of nickel, where, compared with TPR profile I, the presence of Au again lowered the temperature of reduction.

In earlier work [7], we demonstrated (providing a Ni particle size histogram) that the Ni phase in activated Ni/SiO_2–IMP is well dispersed (1–6 nm diameter), with a mean particle size of 1.4 nm, where the particles exhibited a pseudospherical morphology (i.e., no faceting). Selected area electron diffraction (SAED) analysis of Ni/SiO_2–IMP and Ni/TiO_2–IMP confirmed that the Ni phase was present in the metallic form and not as an oxide. The Ni/TiO_2–IMP sample exhibited a similar (even narrower) Ni particle size distribution (mean particle size, 1.2 nm); see Table 2. However, it has been established [36] that the use of ethanediamine precursors to synthesize silica supported Ni catalysts results in the formation of small Ni particles (ca. 2 nm) regardless of Ni loading (up to 20% w/w). The representative TEM image of Ni/TiO_2–IMP given in Fig. 2a reveals particles of near spherical shape but also some evidence of particle faceting.

Table 2
Hydrogen chemisorption, range of metal particle sizes and surface Ni/Au atomic ratios in the activated unused (pre-reaction) and used (post-reaction, after cycles 1 and 2) catalysts

Catalyst	Pre-reaction			Post-reaction	
	H_2 chemisorbed ($\mu mol\ g_{Ni}^{-1}$)	Particle size range (nm)[a]	Ni/Au range	Particle size range (nm)[a]	Ni/Au range
Ni/TiO_2–IMP	702	1–5	–	1–6	–
Ni–Au/TiO_2–IMP	26	3–95	<1–35	3–48	<1–15
Ni–Au/TiO_2–DP	30	2–60	<1–15	5–45	<1–14
Ni/SiO_2–IMP	843	1–6	–	1–8	–
Ni–Au/SiO_2–IMP	18	10–150	<1–40	2–60	1–15

[a] From TEM.

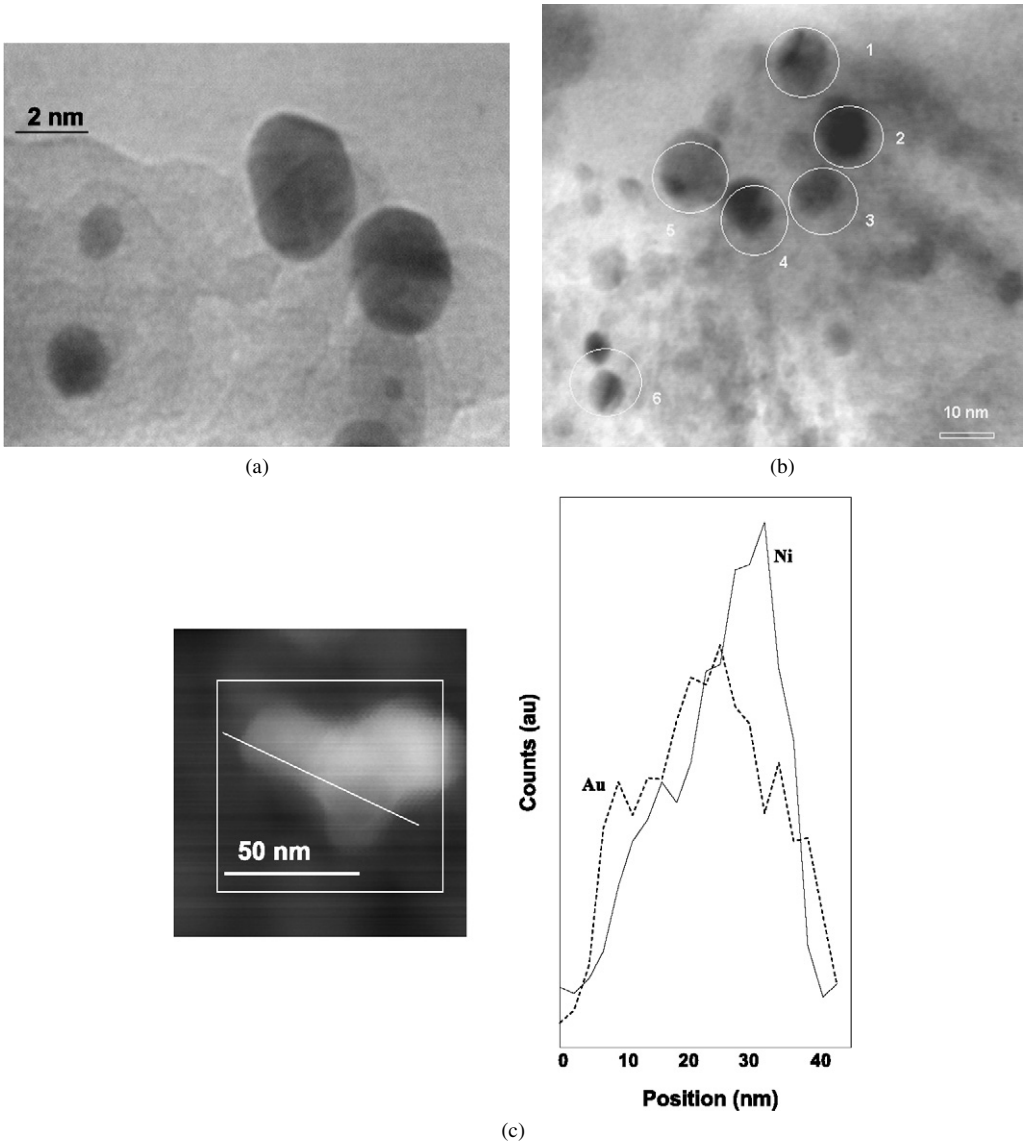

Fig. 2. Representative TEM images of (a) Ni/TiO_2–IMP, (b) Ni–Au/TiO_2–IMP, and (c) STEM annular dark field image of Ni–Au/TiO_2–DP showing a 40 nm segment of sample subjected to EDX mapping with the associated Ni and Au distribution.

Based on repeated and comprehensive TEM analysis, we can assert that Ni particle faceting is a feature of Ni/TiO_2–IMP. The morphology of the supported metal particles is an inherent feature of the associated interfacial energy [43], where faceting is indicative of stronger metal–support interactions, a feature associated with the use of TiO_2 as a support [44,45]. It is worth noting the lower H_2 uptake on Ni/TiO_2–IMP (H/Ni = 0.08) relative to Ni/SiO_2–IMP (H/Ni = 0.1), a response that has been reported previously [46,47] and attributed to suppressed H_2 chemisorption as a result of TiO_2–Ni interaction. Based on a consideration of Ni particle size alone, H_2 chemisorption on Ni/TiO_2–IMP should exceed uptake on Ni/SiO_2–IMP (Table 2).

The metal phase associated with Ni–Au/TiO_2–IMP can be assessed from the representative TEM image given in Fig. 2b. Compared with Ni/TiO_2–IMP, Ni–Au/TiO_2–IMP exhibited a wider range of particle sizes, with metal particles 3–95 nm in diameter; the Ni–Au/SiO_2–IMP sample exhibited an even wider range and larger particle sizes (10–150 nm) (Table 2). This can be attributed in part to the use of a Cl-containing Au precursor. Haruta [33] and Kung et al. [48] have shown that the presence of residual Cl on the surface induces Au particle sintering on thermal treatment, a response that is also a feature of Ni systems [46]. The EDX analyses demonstrate that the particles have a variable Ni–Au composition, as can be seen from the range of Ni/Au atomic ratios reported in Table 2. This is further illustrated by the Ni/Au atomic ratios resulting from EDX analysis of the encircled areas in Fig. 2b for Ni–Au/TiO_2–IMP of 1.5 (area 1), 5.8 (area 2), 4.4 (area 3), 14.1 (area 4), 23.2 (area 5), and 32.1 (area 6). Moreover, the histograms shown in Fig. 3 reveal a broad distribution of Ni/Au ratios for both impregnated bimetallic catalysts. In addition, there was also evidence of significant monometallic Au (10–50 nm) and Ni (8–65 nm) particles in both the Ni–Au/TiO_2–IMP and Ni–Au/SiO_2–IMP samples. In contrast, the Ni–Au/TiO_2–DP sample is characterized by a narrower range of particle sizes (Table 2) and a more uniform distribution of Ni/Au ratios (Fig. 3b)

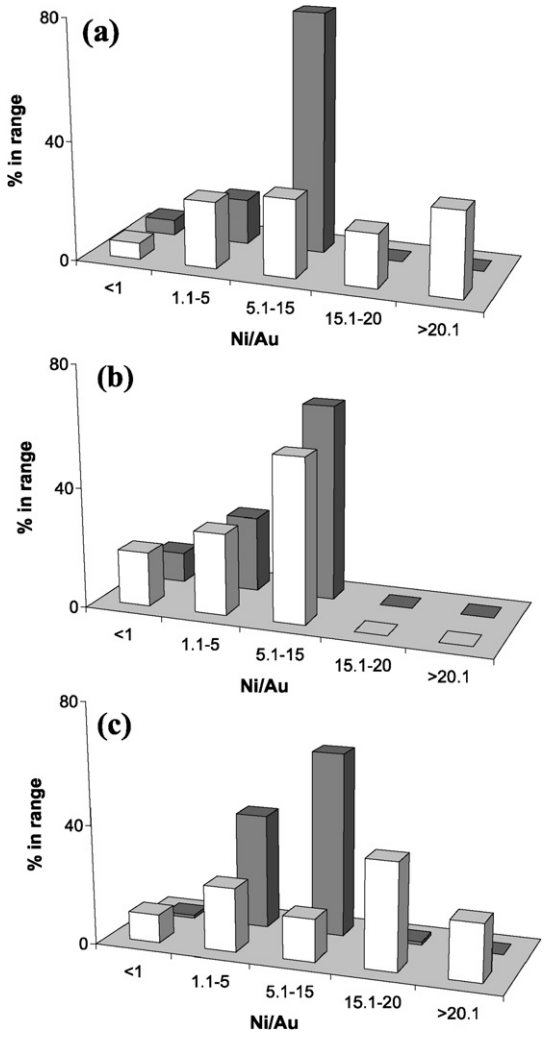

Fig. 3. Surface Ni/Au ratio distribution from EDX analyses of (a) Ni–Au/TiO_2–IMP, (b) Ni–Au/TiO_2–DP, and (c) Ni–Au/SiO_2–IMP pre- (open bars) and post- (solid bars) reaction.

with no monometallic Ni or Au particles. Surface composition of Ni–Au/TiO_2–DP was also probed by EDX mapping along sample lengths of 40–100 nm. A representative analysis is presented in Fig. 2c showing the dark field image with the sample length analyzed and the associated Au and Ni content along this sample segment. It can be seen that the sample bears Au in intimate contact with Ni; the Ni/Au atomic ratio is 0.8–1.9 over the 40-nm section that was mapped.

Whereas the miscibility gap for bulk Au and Ni is such that "bulk alloy" formation is not possible at the temperatures used here, Molenbroek et al. [20] reported "surface" Ni/Au alloy formation in SiO_2- and $MgAl_2O_4$-supported catalysts after reduction at 823 K. Our analyses cannot confirm or discount surface alloy formation, but the TEM-EDX results certainly demonstrate a close proximity of Au to Ni on both SiO_2 and TiO_2 carriers. The H_2 uptake recorded for the three supported bimetallics was significantly lower compared with Ni/TiO_2 and Ni/SiO_2; see Table 2. Bonarowska et al. [16] and Chandler et al. [49] also observed a suppression of H_2 chemisorption for Pd–Au/SiO_2 and Pt–Au/SiO_2, respectively, compared with

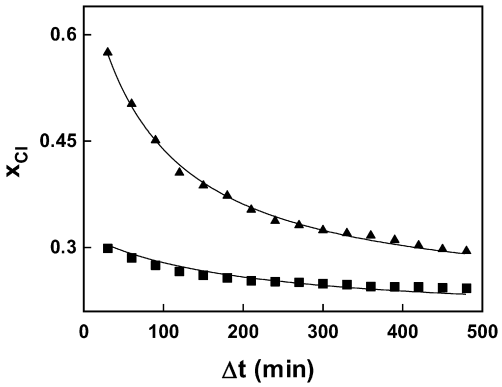

Fig. 4. Fractional dechlorination (x_{Cl}) of 2,4-DCP over Ni/TiO_2–IMP (▲) and Ni/SiO_2–IMP (■). Note: lines represent fits to $(x_{Cl} - x_0)/(x_{480\,min} - x_0) = \Delta t/(\beta + \Delta t)$, correlation coefficients > 0.993.

Pd/SiO_2 and Pt/SiO_2. The nature of the interaction between hydrogen and supported Au systems remains an open question, but it appears that the adsorption capability is limited and dependent on the Au coordination number [50]. Indeed, the lower catalytic hydrogenation activity exhibited by Au catalysts compared with that of Pd or Pt has been generally attributed to an inability of Au surfaces to dissociate molecular H_2, as has been established in experimental [51] and theoretical studies [8]. Nevertheless, several authors have observed an unexpected dissociative chemisorption of H_2 (or D_2) on Au films containing defective sites [52–54]. Moreover, in the case of supported gold nanoparticles, dissociation of hydrogen seems to occur on the low-coordinated sites of gold particles (edges and corners) [11,55]. For Au/TiO_2, the dissociation of hydrogen on Au particles has been proposed as the rate-determining step in the hydrogenation of crotonaldehyde [11], and a combination of in situ X-ray absorption spectroscopy, chemisorption, and H/D exchange experiments have demonstrated that H_2 is dissociatively adsorbed on Au/Al_2O_3 [55]. In the present study, we recorded H_2 uptake on both monometallic Au samples of <3 μmol g_{Au}^{-1}, which is close to the instrumental detection limits. The appreciably lower H_2 uptakes recorded for the bimetallic catalysts compared with the Ni catalysts suggests some surface Ni–Au interaction that inhibits H_2 chemisorption on Ni; the consequences of this in terms of catalytic HDC are considered below.

3.2. Catalytic response

In this study, the HDC of 2,4-dichlorophenol (2,4-DCP) generated 2-chlorophenol (2-CP) and 4-chlorophenol (4-CP) as partially dechlorinated products and phenol as the ultimate dechlorination product. No evidence of any significant aromatic ring reduction was found; only trace quantities (<2% conversion) of cyclohexanol and cyclohexanone were isolated in the product stream at $\Delta t < 30$ min. Fig. 4 illustrates fractional HDC (x_{Cl}) as a function of TOS for reaction over Ni/TiO_2–IMP and Ni/SiO_2–IMP. Both cases exhibited a temporal drop in the level of HDC, which can be expressed in terms of the empirical relationship

$$\frac{(x_{Cl} - x_0)}{(x_{480\,min} - x_0)} = \frac{\Delta t}{(\beta + \Delta t)}.$$

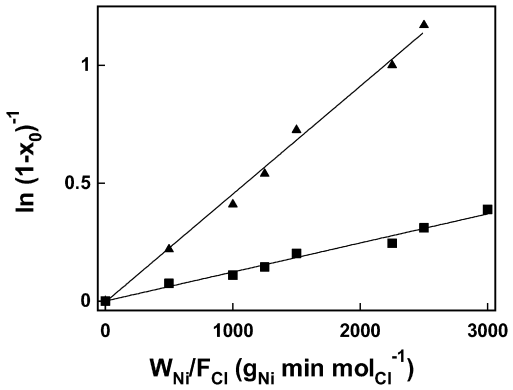

Fig. 5. Pseudo-first-order kinetic plots for the HDC of 2,4-DCP over Ni/TiO_2–IMP (▲) and Ni/SiO_2–IMP (■).

Fit convergence yields values for x_0, the initial fractional HDC, where $x_{480\ \mathrm{min}}$ represents the fractional conversion at the end of the run (480 min) and β is a time scale-fitting parameter. Plug-flow operation, with hydrogen maintained far in excess, yielded the following applicable reactor/kinetic expression [27]:

$$\ln\left(\frac{1}{1-x_0}\right) = k\left(\frac{W}{F_{\mathrm{Cl}}}\right),$$

where F_{Cl} is the inlet molar Cl feed rate and the parameter W/F_{Cl} (units, g min $\mathrm{mol}_{\mathrm{Cl}}^{-1}$) has the physical significance of contact time. From a consideration of gas-phase reaction equilibrium constants [28], HDC under the stated reaction conditions can be considered irreversible. Fig. 5 shows representative linear plots of $\ln(1-x_0)^{-1}$ versus $W_{\mathrm{Ni}}/F_{\mathrm{Cl}}$ generated for 2,4-DCP HDC over Ni/TiO_2–IMP and Ni/SiO_2–IMP, where both lines can be seen to pass through the origin, indicating adherence to pseudo-first-order kinetics. Table 3 provides the specific initial rate constants extracted from this pseudo-first-order treatment, which demonstrate that Ni/TiO_2–IMP delivered an appreciably higher HDC rate than Ni/SiO_2–IMP.

Some consensus is emerging from the literature that catalytic hydrodehalogenation is structure-sensitive, dependent on metal particle size and electronic structure [29,56–60]. Because both supported monometallic Ni catalysts exhibit similar Ni size distributions and mean particle sizes, a stronger metal–support interaction in the case of Ni/TiO_2–IMP through electronic effects must contribute to the generation of an intrinsically more efficient HDC catalyst. Indeed, it has been demonstrated elsewhere [61] that the electron density of Ni crystallites supported on TiO_2 is appreciably greater than that associated with Ni on SiO_2. This increased electron density can have an appreciable effect in "electronic-sensitive" hydrogenolysis reactions, in which turnover frequency can vary by orders of magnitude depending on metal site electron density [45]. Indeed, Aristizabal et al. [62] also recorded higher activities in the H_2-mediated dechlorination of dichloromethane over TiO_2-supported Pd and Ni relative to silica-based systems. Urbano and Marinas, in their review of catalytic HDC [63] systems, identified a number of instances in which metal–support interactions affected overall performance, most notably in terms of minimizing deactivation. Nonetheless, it should be noted that Coq et al. [64] observed a decrease in chlorobenzene HDC activity for smaller (electron-deficient) Pd particles supported on alumina. Gampine and Eyman [65] linked support effects in HDC reactions to possible substrate–reactant interactions, and C–Cl bond activation can be facilitated through DCP (or CP) interaction with the oxygen vacancies of titania [62]. The involvement of spillover hydrogen in catalytic HDC [66,67] is a further consideration, where the nature of the accepting oxide support can have a significant influence on hydrogen transfer, as can the presence of residual surface Cl [68]. The nature of the support is known to influence HDC selectivity [69], and it is significant that Ni/TiO_2–IMP generated both CP isomers, whereas 2-CP was the sole partially dechlorinated product for reaction over Ni/SiO_2–IMP (Table 3). In substituted aromatic systems, reactivity is typically related to localized (inductive) and delocalized (resonance) effects [70]. When the Cl substituents are positioned *meta* to each other, as in the case of 2,4-DCP, the arenium intermediates for attack at either Cl are equally stable, with the result that HDC should generate equal proportions of 2-CP and 4-CP [28]. The sole production of 2-CP over Ni/SiO_2–IMP suggests an overriding steric hindrance effect in which the *ortho*-positioned Cl substituent is less susceptible to attack, whereas resonance effects appear to contribute to HDC over Ni/TiO_2–IMP, presumably through reactant–support interactions.

Reaction over both Au/TiO_2 and Au/SiO_2 delivered negligible HDC activity ($x_{\mathrm{Cl}} < 0.03$) to generate CP with no detectable phenol formation. Such limited HDC activity can be linked to the low associated H_2 uptake recorded for these samples. Earlier [7], we reported that the addition of gold to Ni/SiO_2–IMP increased HDC activity, a response confirmed by the HDC rate constants given in Table 3. This effect also extends, albeit to a lesser extent (in reaction cycle 1), to Ni–Au co-impregnated titania. Because the monometallic Au catalysts exhibited negligi-

Table 3
Specific pseudo-first-order 2,4-DCP HDC rate constants (see Fig. 5) and the initial selectivity to 2-CP ($S_{2\text{-CP}}$), 4-CP ($S_{4\text{-CP}}$), and phenol (S_{phenol}) over the two reaction cycles; $W_{\mathrm{Ni}}/F_{\mathrm{Cl}} = 2500\ g_{\mathrm{Ni}}\ \mathrm{mol}_{\mathrm{Cl}}^{-1}$ min; $W_{\mathrm{Au}}/F_{\mathrm{Cl}} = 820\ g_{\mathrm{Au}}\ \mathrm{mol}_{\mathrm{Cl}}^{-1}$ min

Catalyst	Reaction cycle 1				Reaction cycle 2			
	$10^4 k$ ($\mathrm{mol_{Cl}\ g_{Ni}^{-1}\ min^{-1}}$)	$S_{2\text{-CP}}$ (%)	$S_{4\text{-CP}}$ (%)	S_{phenol} (%)	$10^4 k$ ($\mathrm{mol_{Cl}\ g_{Ni}^{-1}\ min^{-1}}$)	$S_{2\text{-CP}}$ (%)	$S_{4\text{-CP}}$ (%)	S_{phenol} (%)
Ni/TiO_2–IMP	4.6	17	8	75	3.3	18	13	69
Ni–Au/TiO_2–IMP	5.2	14	6	80	8.7	10	0	90
Ni–Au/TiO_2–DP	9.8	6	0	94	11.6	8	0	92
Ni/SiO_2–IMP	1.3	22	0	78	1.1	23	0	77
Ni–Au/SiO_2–IMP	3.2	30	0	70	7.7	13	0	87

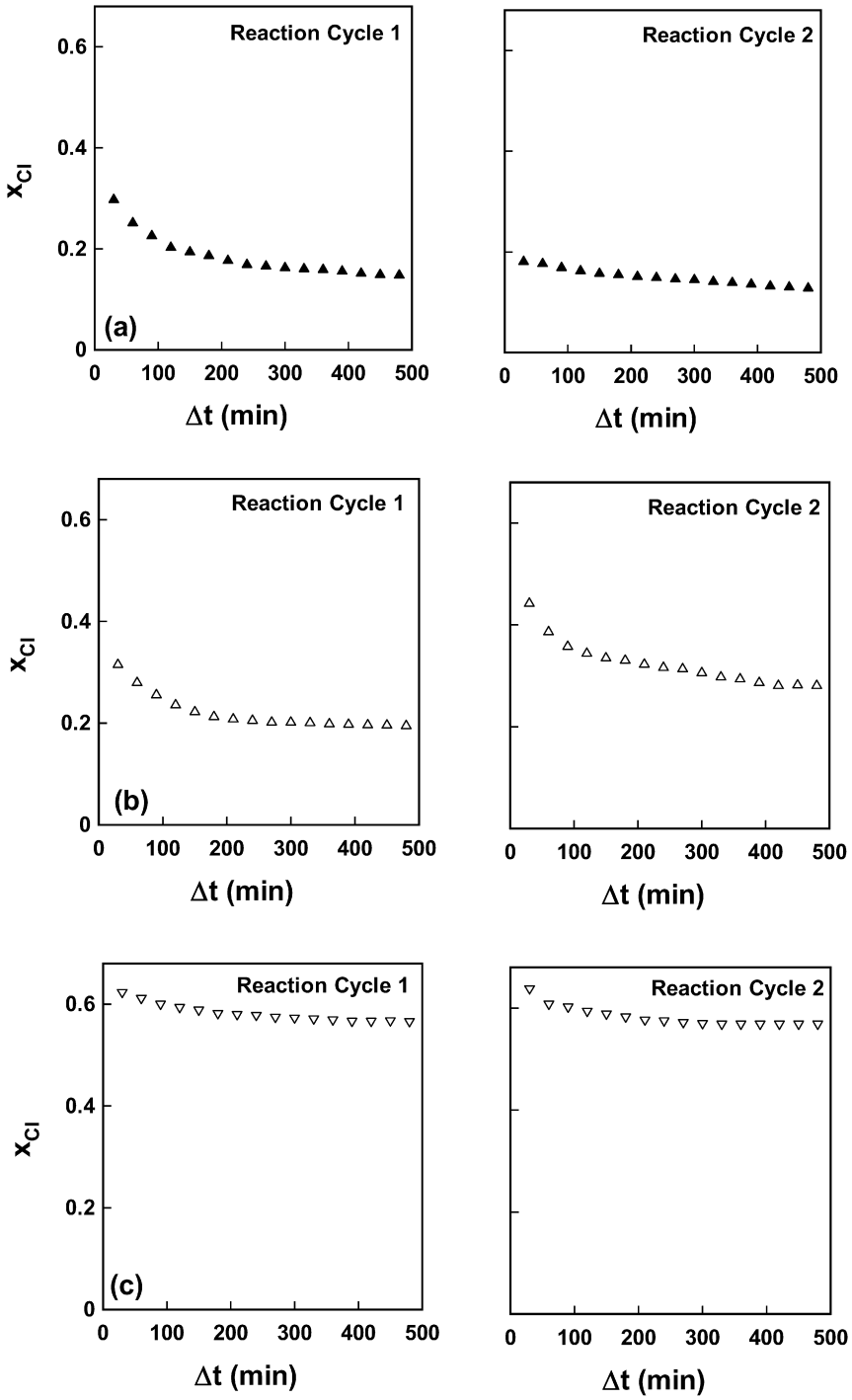

Fig. 6. Variation of fractional 2,4-DCP dechlorination (x_{Cl}) with time-on-stream in reaction cycle 1 and reaction cycle 2 over (a) Ni/TiO_2–IMP (▲), (b) Ni–Au/TiO_2–IMP (△), (c) Ni–Au/TiO_2–DP (▽), (d) Ni/SiO_2–IMP (■), and (e) Ni–Au/SiO_2–IMP (□): $W_{Ni}/F_{Cl} = 1000\ g_{Ni}\ mol_{Cl}^{-1}$ min; $W_{Au}/F_{Cl} = 330\ g_{Au}\ mol_{Cl}^{-1}$ min.

ble activity under the same reaction conditions, any measurably enhanced HDC performance associated with the bimetallics must be the result of some surface Au–Ni synergy. It is intriguing that the lower H_2 uptake associated with the bimetallics did not result in a net reduction in HDC activity. The promotional effect may have had a geometric and/or electronic source in which particle size and composition are critical. In HDC applications over supported bimetallics [63], a close contact between Pd and a second metal (if not alloy formation) has been deemed essential for any significant catalytic response. It is significant that the Ni–Au/TiO_2–DP sample, which had the narrowest Ni/Au ratio distribution and the smallest metal particles (Fig. 3b), generated the highest HDC rate constant. The Au component may make a direct contribution to the HDC reaction through activation of the C–Cl bond with subsequent attack from reactive hydrogen dissociated at the Ni centers, a mechanism that has been proposed by Venezia et al. for the hydrodesulfurization of thiophene over Pd–Au/SiO_2 [18].

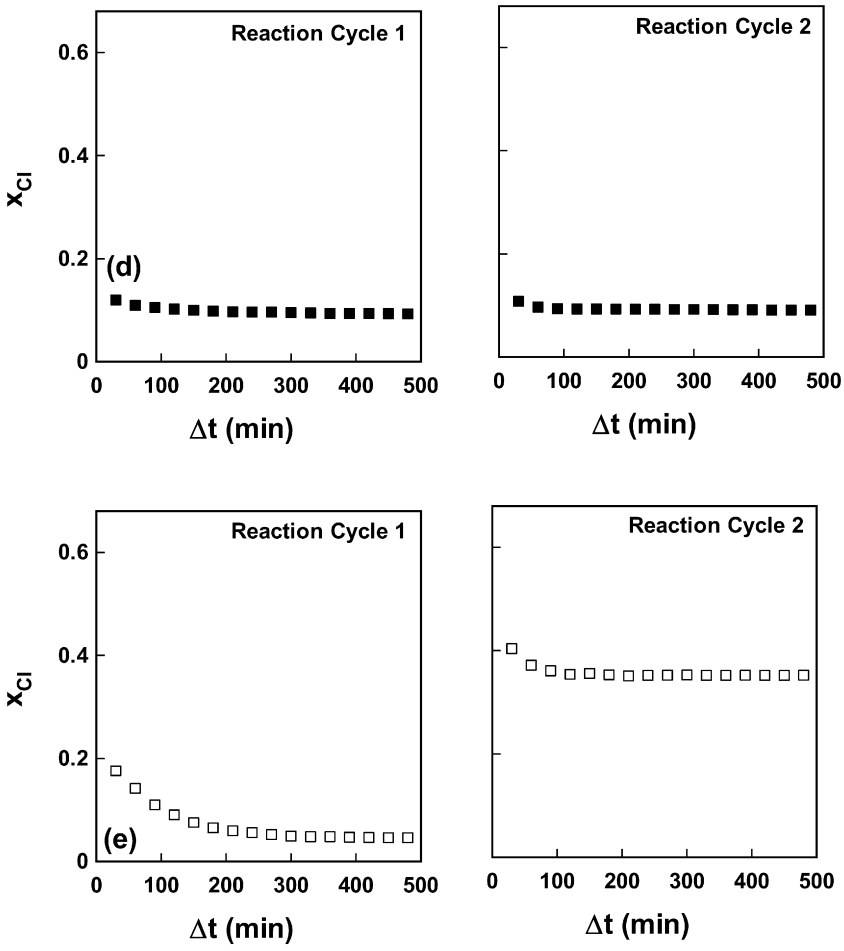

Fig. 6. (*continued*)

Moreover, Heinrichs et al. [71] have explained the selectivity response that they observed for the dechlorination of 1,2-dichloroethane over Pd–Ag/SiO_2 by assuming Cl interaction at the Ag sites, where Pd serves as a source of reactive hydrogen.

Fig. 6 illustrates variations in fractional dechlorination (x_{Cl}) as a function of TOS over two reaction cycles for all of the catalysts. The temporal decline in HDC activity (shown in Fig. 4) is again evident to varying degrees. Such a decline has been observed for related catalytic HDC systems and attributed to carbon deposition/occlusion of the active metal sites and/or surface poisoning by HCl and/or metal sintering [22]. In Ni/TiO_2–IMP and Ni/SiO_2–IMP, resumption of the reaction after H_2 thermal treatment (reaction cycle 2) gave x_{Cl} values comparable to those obtained at the conclusion of the previous reaction cycle, with a subsequent gradual decline with TOS. The initial HDC rate constants (recorded in Table 3) were lower for cycle 2, indicating TOS-irreversible catalyst deactivation. In complete contrast, thermal treatment resulted in an increase in HDC activity associated with Ni–Au/TiO_2–IMP and Ni–Au/SiO_2–IMP, with an associated increase in the k values by a factor of up to 2.4. Such an effect was not as apparent for Ni–Au/TiO_2–DP (the most active catalyst), for which the activity profiles for reaction cycles 1 and 2 are similar but a measurable increase in HDC rate constant was seen for cycle 2 (see Table 3). The catalytic response in terms of partial versus complete HDC, quantified by the selectivity with respect to CP (2-CP + 4-CP) and phenol, can be assessed based on the TOS selectivity responses plotted in Fig. 7. The temporal decline in x_{Cl} over reaction cycle 1 (see Fig. 6) is accompanied by an increasing preferential partial dechlorination with a consequent TOS increase in CP selectivity (Fig. 7). The reaction selectivity in cycle 2 for Ni/TiO_2–IMP and Ni/SiO_2–IMP was essentially that attained at the completion of cycle 1. As a direct corollary to the increased HDC rate constant after thermal treatment over the impregnated bimetallics, CP selectivity was decreased in favor of complete dechlorination to phenol, a response that was especially marked for Ni–Au/SiO_2–IMP (see Fig. 7e). The thermal treatment after reaction cycle 1 had an additional impact on the prevailing HDC pathway over Ni–Au/TiO_2–IMP, in that no 4-CP was formed in reaction cycle 2 (see Table 3).

In the cases of Ni/TiO_2–IMP over both reaction cycles and Ni–Au/TiO_2–IMP over cycle 1, the [4-CP]/[2-CP] ratio in the product mixture increased with increasing TOS. This temporal dependence of selectivity, shown in Fig. 8, suggests a contribution due to the HCl produced that induces a preferential hydrogenolysis of the *ortho*-Cl substituent through surface interactions. The most active Ni–Au/TiO_2–DP sample exhibited little change in the temporal selectivity variation in either cycle, where phenol formation was overwhelmingly preferred.

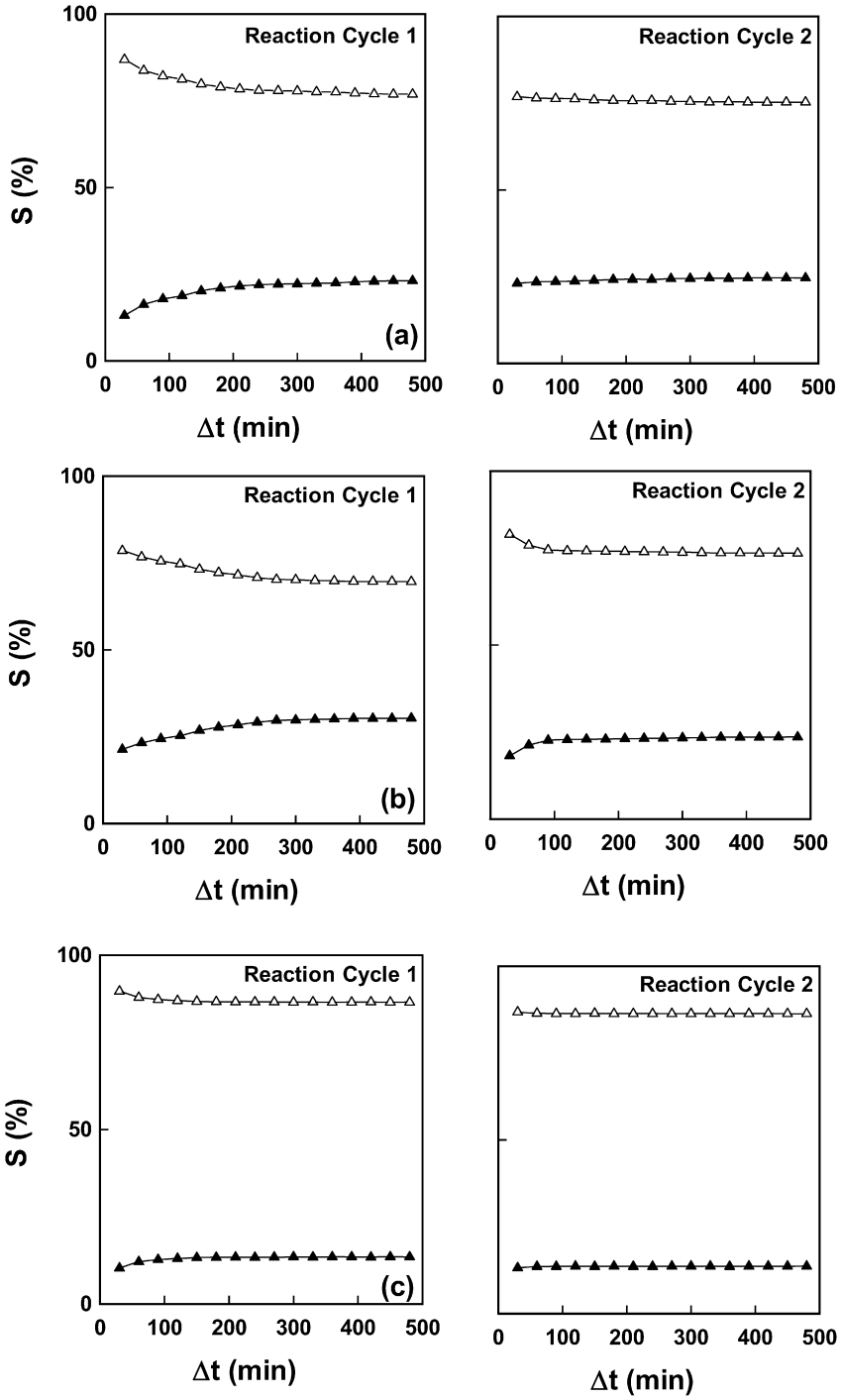

Fig. 7. Variation of product selectivity (S) in terms of CP (2-CP + 4-CP) (▲) and phenol (△) production with time-on-stream in reaction cycle 1 and reaction cycle 2 over (a) Ni/TiO_2–IMP, (b) Ni–Au/TiO_2–IMP, (c) Ni–Au/TiO_2–DP, (d) Ni/SiO_2–IMP, and (e) Ni–Au/SiO_2–IMP: $W_{Ni}/F_{Cl} = 1000$ g_{Ni} mol_{Cl}^{-1} min; $W_{Au}/F_{Cl} = 330$ g_{Au} mol_{Cl}^{-1} min.

3.3. Catalyst characterization after reaction

Because the catalysts exhibited distinct variations in HDC activity/selectivity before (reaction cycle 1) and after reaction/thermal treatment (reaction cycle 2), the used catalysts were also subjected to characterization analyses to account for the difference in catalytic performance. Although no apparent change in Ni particle morphology in the monometallic catalysts was seen post-HDC, a definite broadening of Ni particle size distribution (Table 2) was detected (mean Ni size, 2.1 nm for Ni/SiO_2–IMP and 1.5 nm for Ni/TiO_2–IMP). This effect can be ascribed to a halide-induced agglomeration of Ni particles due to the surface mobility of Ni–Cl species [10]. In marked contrast, after both reaction cycles, the bimetallic catalysts exhibited a narrower size range, as did the surface Ni/Au atomic ratios. This is demonstrated by the TEM image given in Fig. 9

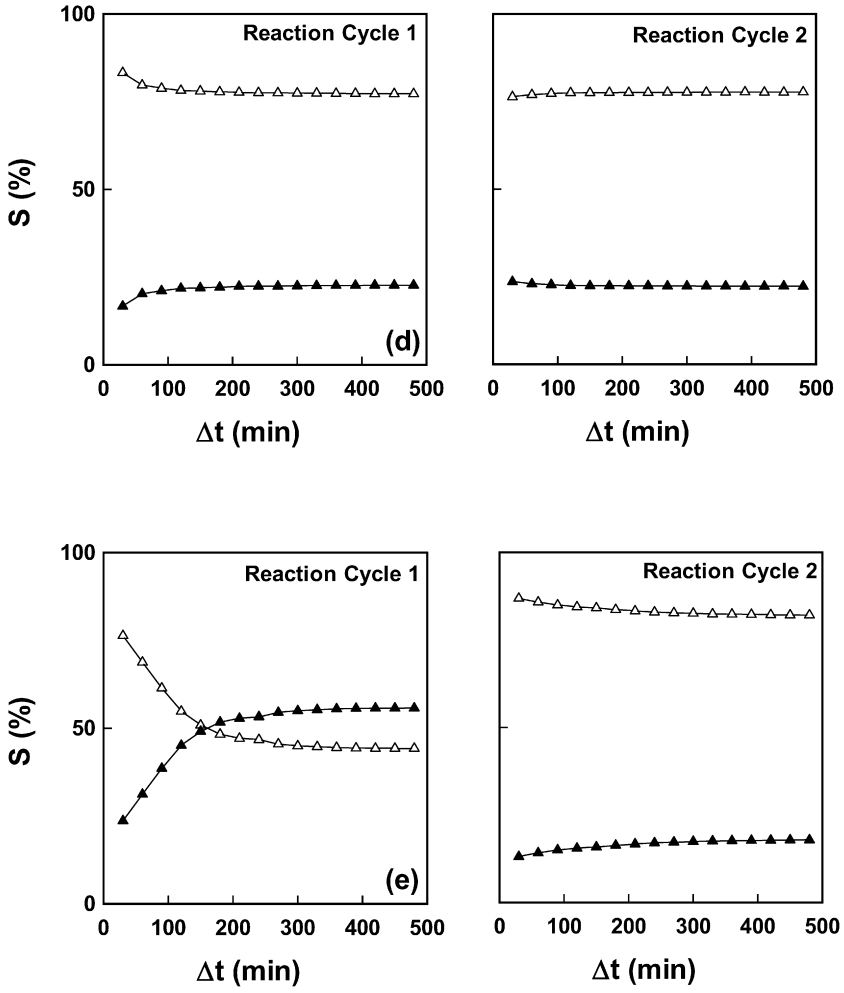

Fig. 7. (*continued*)

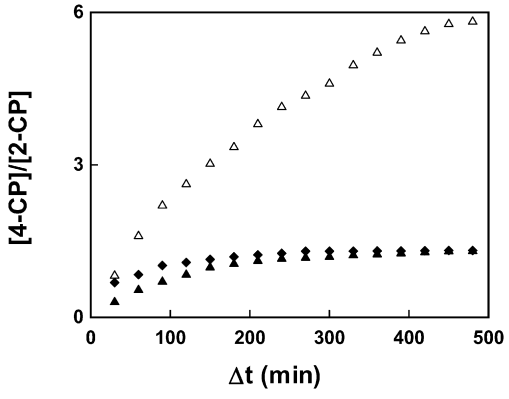

Fig. 8. Ratio of [4-CP] to [2-CP] in the product stream as a function of time-on-stream for reaction over Ni/TiO_2–IMP (▲, reaction cycle 1 and ◆, reaction cycle 2) and Ni–Au/TiO_2–IMP (△, reaction cycle 1): $W_{Ni}/F_{Cl} = 1000$ $g_{Ni}\,mol_{Cl}^{-1}$ min; $W_{Au}/F_{Cl} = 330$ $g_{Au}\,mol_{Cl}^{-1}$ min.

that takes Ni–Au/TiO_2–IMP as a representative case, showing a smaller particle size characterized by a narrower Ni/Au range. Fig. 9 also presents EDX analysis results for the encircled areas. As we found in our earlier study of Ni–Au/SiO_2–IMP [7], there was no evidence of discrete Ni and Au monometallic particles in Ni–Au/TiO_2–IMP postreaction. The shift in Ni/Au surface ratios to smaller values can also be assessed from the histogram entries in Fig. 3. The increase in HDC activity that resulted from combined reaction/thermal treatment must be due to a surface restructuring, leading to a more homogeneous combination of Ni and Au in smaller particles. It is significant that the surface characteristics of the Ni–Au/TiO_2–DP catalyst were not drastically altered over the two reaction cycles, a response that can be linked to the relative insensitivity of the associated HDC rate constant/selectivities (Table 3). Taking an overview of the TEM-EDX and catalysis results, it appears that a preponderance of metal particles with Ni/Au ratios in the 5–15 range enhances HDC performance.

4. Conclusions

The findings reported in this paper support the following conclusions:

(1) Although Ni/TiO_2–IMP and Ni/SiO_2–IMP exhibited a similar Ni particle size distribution (1–6 nm) and mean size (1.2–1.4 nm), Ni/TiO_2–IMP delivered a higher specific HDC rate constant than Ni/SiO_2–IMP and generated significant quantities of 4-CP (as well as 2-CP and phenol) in the

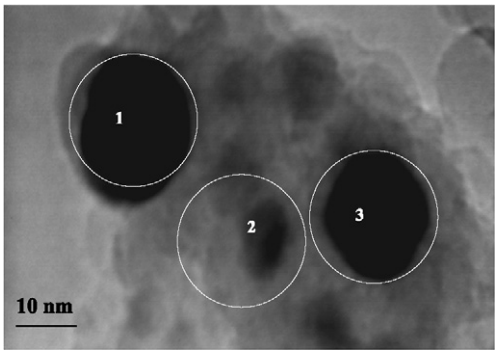

Fig. 9. Representative TEM image of Ni–Au/TiO_2–IMP post-reaction (after reaction cycle 1 and reaction cycle 2) where EDX analysis of the encircled areas delivered Ni/Au atomic ratios = 9.4 (area 1), 11.2 (area 2), and 6.3 (area 3).

product stream, whereas reaction over Ni/SiO_2–IMP generated only 2-CP and phenol. The difference in HDC activity and selectivity implies a support effect. This response is attributed to Ni–TiO_2 interactions that modify Ni site electron density to generate an intrinsically more efficient HDC catalyst. The sole production of 2-CP (as a partially dechlorinated product) over Ni/SiO_2–IMP indicates an overriding steric-hindering contribution, whereas the production of 4-CP over Ni/TiO_2–IMP (and Ni–Au/TiO_2–IMP) suggests the involvement of resonance effects, possibly due to reactant–support interactions.

(2) Activation of co-impregnated Ni–Au on both supports generated much larger metal particles (3–150 nm) due to the presence of Cl in the Au precursor, which causes sintering during reduction, with a variable Ni/Au surface composition (<1–40 nm) and poorly dispersed segregated Au (10–50 nm) and Ni (8–65 nm) particles.

(3) Preparation of the TiO_2-supported bimetallic by co-deposition–precipitation generated a narrower range of particle sizes (2–60 nm) and a more uniform Ni/Au distribution (<1–15) with no detectable segregated Ni or Au particles. The presence of Au, regardless of the support or synthesis route, served to lower Ni^{II} reduction temperature but resulted in suppression of Ni H_2 chemisorption capacity.

(4) HDC over Au/TiO_2 and Au/SiO_2 resulted in negligible activity ($x_{Cl} < 0.03$) to generate CP with no detectable phenol formation. However, each bimetallic exhibited higher HDC rate constants than the corresponding Ni monometallic, suggesting some Ni–Au surface synergism that enhanced HDC performance. It is tentatively proposed that the Au component serves to activate the C–Cl bond with subsequent attack from reactive hydrogen dissociated at the Ni centers. The Ni–Au/TiO_2–DP sample, which had the narrowest surface Ni/Au ratio distribution and the smallest metal particles, generated the highest HDC rate constant.

(5) H_2 thermal treatment of the bimetallic catalysts postreaction (reaction cycle 1) resulted in surface restructuring leading to a better dispersion of Ni/Au clusters (2–60 nm) bearing a narrower Ni/Au composition (<1–15). During reaction cycle 2, this restructuring was accompanied by an increase in the HDC rate constant and high selectivities to phenol (>85%); that is, complete dechlorination. In contrast, the monometallic samples exhibited irreversible deactivation with repeated use. HDC performance is sensitive to surface Ni/Au composition and is enhanced when either the method of preparation or sample treatment ensures intimate Ni–Au contact and a more homogeneous surface Ni/Au composition.

Acknowledgments

The contributions to this work by Wenqin Shen, Javier Lopez, Olivier Dargaud, and Alan Dozier are gratefully acknowledged.

References

[1] M. Haruta, T. Kobayashi, H. Sano, N. Yamada, Chem. Lett. (1987) 405.
[2] C.W. Corti, R.J. Holliday, D.T. Thomson, Appl. Catal. A Gen. 291 (2005) 253.
[3] G.C. Bond, Gold Bull. 34 (2001) 117.
[4] G.J. Hutchings, M. Haruta, Appl. Catal A Gen. 291 (2005) 2.
[5] M. Besson, A. Kallel, P. Gallezot, R. Zanella, C. Louis, Catal. Commun. 4 (2003) 471.
[6] A. Ueda, T. Ohshima, M. Haruta, Appl. Catal. B Environ. 12 (1997) 81.
[7] G. Yuan, J. Lopez, C. Louis, L. Delannoy, M.A. Keane, Catal. Commun. 6 (2005) 555.
[8] B. Hammer, J.K. Norskov, Nature 376 (1995) 238.
[9] J. Jia, K. Haraki, J.N. Kondo, K. Domen, K. Tamaru, J. Phys. Chem. B 104 (2000) 11153.
[10] M. Okumura, T. Akita, M. Haruta, Catal. Today 74 (2002) 265.
[11] R. Zanella, C. Louis, S. Giorgio, R. Touroude, J. Catal. 223 (2004) 328.
[12] L. Guczi, Catal. Today 101 (2005) 53.
[13] T.V. Choudhary, C. Sivadinarayana, A.K. Datye, D. Kumar, D.W. Goodman, Catal. Lett. 86 (2003) 1.
[14] M. Bonarowska, B. Burda, W. Juszczyk, J. Pielaszek, Z. Kowalczyk, Z. Karpinski, Appl. Catal. B Environ. 35 (2001) 13.
[15] M. Bonarowska, J. Pielaszek, V.A. Semikolenov, Z. Karpinski, J. Catal. 209 (2002) 528.
[16] M. Bonarowska, A. Malinowski, W. Juszczyk, Z. Karpinski, Appl. Catal. B Environ. 30 (2001) 187.
[17] M.O. Nutt, J.B. Hughes, M.S. Wong, Environ. Sci. Technol. 39 (2005) 1346.
[18] A.M. Venezia, V. La Parola, G. Deganello, B. Pawlec, J.L.G. Fierro, J. Catal. 215 (2003) 317.
[19] F. Besenbacher, I. Chorkendorff, B.S. Clausen, B. Hammer, A.M. Molenbroek, J.K. Norskov, I. Stensgaard, Science 279 (1998) 1913.
[20] A.M. Molenbroek, J. Nørskov, B.S. Clausen, J. Phys. Chem. B 105 (2001) 105.
[21] N.C. Triantafyllopoulos, S.C. Neophytides, J. Catal. 239 (2006) 187.
[22] M.A. Keane, in: M.A. Keane (Ed.), Interfacial Applications in Environmental Engineering, Dekker, New York, 2003, p. 231, chap. 13.
[23] R.K. Juhler, S.R. Sorensen, L. Larsen, Water Res. 35 (2001) 1371.
[24] J.K. Fawell, S. Hunt, Environmental Toxicology: Organic Pollutants, Ellis Horwood, Chichester, 1988.
[25] G. Tavoularis, M.A. Keane, J. Mol. Catal. A Chem. 142 (1999) 187.
[26] G. Tavoularis, M.A. Keane, J. Chem. Technol. Biotechnol. 74 (1999) 60.
[27] M.A. Keane, Appl. Catal. A Gen. 271 (2004) 109.
[28] E.-J. Shin, M.A. Keane, Chem. Eng. Sci. 54 (1999) 1109.
[29] G. Pina, C. Louis, M.A. Keane, Phys. Chem. Chem. Phys. 5 (2003) 1924.
[30] B.P. Block, J.C. Bailar Jr., J. Am. Chem. Soc. 73 (1951) 4722.
[31] P. Burattin, M. Che, C. Louis, J. Phys. Chem. B 101 (1997) 7060.
[32] R. Zanella, S. Giorgio, C. Henry, C. Louis, J. Phys. Chem. B 106 (2002) 7634.
[33] M. Haruta, CATTECH 6 (2002) 102.
[34] L. Delannoy, N. El-Hassan, A. Musi, L.T.N. Nguyen, J.-M. Krafft, C. Louis, J. Phys. Chem. B 110 (2006) 22471.

[35] G. Yuan, M.A. Keane, Chem. Eng. Sci. 58 (2003) 257.
[36] Z.X. Cheng, C. Louis, M. Che, Stud. Surf. Sci. Catal. 91 (1995) 1027.
[37] D. Guillemot, Ph.D. dissertation, Université Paris VI, 1997.
[38] R. Zanella, L. Delannoy, C. Louis, Appl. Catal. A Gen. 291 (2005) 62.
[39] L.I. Ilieva, D.H. Andreeva, A.A. Andreev, Thermochim. Acta 292 (1997) 169.
[40] A. Venugopal, M.S. Scurrell, Appl. Catal. A Gen. 258 (2004) 241.
[41] D. Andreeva, V. Idakiev, T. Tabakova, L. Ilieva, P. Falaras, A. Bourlinos, A. Travlos, Catal. Today 72 (2002) 51.
[42] G. Munteanu, L. Ilieva, R. Nedyalkova, D. Andreeva, Appl. Catal. A Gen. 277 (2004) 31.
[43] R.T.K. Baker, J. Catal. 63 (1980) 523.
[44] A.Y. Stakheev, L.M. Kustov, Appl. Catal. A Gen. 188 (1999) 3.
[45] E. Ruckenstein, H.Y. Wang, J. Catal. 190 (2000) 32.
[46] C. Hoang-Van, Y. Kachaya, S.J. Teichner, Y. Arnaud, J.A. Dalmon, Appl. Catal. 46 (1989) 281.
[47] M.C.J. Bradford, M.A. Vannice, Appl. Catal. A Gen. 142 (1996) 73.
[48] H.H. Kung, M.C. Kun, C.K. Costello, J. Catal. 216 (2003) 425.
[49] B.D. Chandler, A.B. Schabel, L.P. Pignoulet, J. Phys. Chem. B 105 (2001) 149.
[50] P. Claus, Appl. Catal. A Gen. 291 (2005) 222.
[51] A.G. Sault, R.J. Madix, C.T. Cambell, Surf. Sci. 169 (1986) 347.
[52] M. Okada, S. Ogura, W. Agerico Dino, M. Wilde, K. Fukutani, T. Kasai, Appl. Catal. A Gen. 291 (2005) 55.
[53] M. Okada, M. Nakamura, K. Moritani, T. Kasai, Surf. Sci. 523 (2003) 218.
[54] L. Stobinski, L. Zommer, R. Dus, Appl. Surf. Sci. 141 (1999) 319.
[55] E. Bus, J.T. Miller, J.A. van Bokhoven, J. Phys. Chem. B 109 (2005) 14581.
[56] S.B. Halligudi, B.M. Devassay, A. Ghosh, V. Ravikumar, J. Mol. Catal. A Chem. 184 (2002) 175.
[57] Z. Karpinski, K. Early, J.L. d'Itri, J. Catal. 164 (1996) 378.
[58] A.R. Suzdorf, S.V. Morozov, N.N. Anshits, S.I. Tsiganova, A.G. Anshits, Catal. Lett. 29 (1994) 49.
[59] M.A. Keane, C. Park, C. Menini, Catal. Lett. 88 (2003) 89.
[60] L.N. Zanaveskin, V.A. Aver'yanov, Yu.A. Treger, Russ. Chem. Rev. 65 (1996) 617.
[61] B. Imelik, J.C. Vedrine, Catalyst Characterisation, Physical Techniques for Solid Materials, Plenum, New York, 1994.
[62] B. Aristizabal, C.A. Gonzalez, I. Barrio, M. Montes, C. Montes de Correa, J. Mol. Catal. A Chem. 222 (2004) 189.
[63] F.J. Urbano, J.M. Marinas, J. Mol. Catal. A Chem. 173 (2001) 329.
[64] B. Coq, G. Ferrat, F. Figueras, J. Catal. 101 (1986) 434.
[65] A. Gampine, D.P. Eyman, J. Catal. 179 (1998) 315.
[66] M.A. Keane, G. Tavoularis, React. Kinet. Catal. Lett. 78 (2003) 11.
[67] L.M. Gomez-Sainero, A. Cortes, X.L. Seoane, A. Arcoya, Ind. Eng. Chem. Res. 39 (2000) 2849.
[68] W.C. Conner Jr., J.L. Falconer, Chem. Rev. 95 (1995) 759.
[69] B. Coq, F. Francois, Coord. Chem. Rev. 178–180 (1998) 1753.
[70] W.H. Brown, Organic Chemistry, Saunders College Publ., New York, 1995.
[71] B. Heinrichs, P. Delhez, J.P. Schoebrechts, J.P. Pirard, J. Catal. 172 (1997) 322.